IEEE Access
Multidisciplinary | Rapid Review | Open Access Journal

Received August 16, 2019, accepted September 10, 2019, date of publication September 13, 2019, date of current version October 1, 2019.

Digital Object Identifier 10.1109/ACCESS.2019.2941257

An Efficient Multilevel Fast Multipole Algorithm to Solve Volume Integral Equation for Arbitrary Inhomogeneous Bi-Anisotropic Objects

JINBO LIU[1], ZENGRUI LI[1], (Member, IEEE), LIMEI LUO[1], AND JIMING SONG[2], (Fellow, IEEE)

[1]School of Information and Communication Engineering, Communication University of China, Beijing 100024, China
[2]Department of Electrical and Computer Engineering, Iowa State University, Ames, IA 50011, USA

Corresponding author: Zengrui Li (zrli@cuc.edu.cn)

This work was supported in part by the National Natural Science Foundation of China under Grant 61701447, Grant 61671415, and Grant 61331002, and in part by the Fundamental Research Funds for the Central Universities under Grant CUC19ZD001 and Grant CUC2019B068.

ABSTRACT A volume integral equation (VIE) based on the mixed-potential representation is presented to analyze the electromagnetic scattering from objects involving inhomogeneous bi-anisotropic materials. By discretizing the objects using tetrahedrons on which the commonly used Schaubert-Wilton-Glisson (SWG) basis functions are defined, the matrix equation is derived using the method of moments (MoM) combined with the Galerkin's testing. Further, adopting an integral strategy of tetrahedron-to-tetrahedron scheme, the multilevel fast multipole algorithm (MLFMA) is proposed to accelerate the iterative solution, which is further improved by using the spherical harmonics expansion with a faster implementation and low memory requirement. The memory requirement of the radiation patterns of basis functions in the proposed MLFMA is several times less than that in the conventional MLFMA.

INDEX TERMS Bi-anisotropy, method of moments (MoM), multilevel fast multipole algorithm (MLFMA), spherical harmonics expansion, volume integral equation (VIE).

I. INTRODUCTION

With the rapid development of material science, the electromagnetic (EM) radiation or scattering properties of complicated materials have aroused great interests in the field of computational electromagnetics. Lots of researches focus on the anisotropic or bi-anisotropic materials since their wide applications, such as the applications in microwave and millimeter-wave devices, radar absorbers, EM stealth, and so on [1]–[4]. However, because the constitutive relations of the bi-anisotropic materials are enforced an additional coupling between the electric and magnetic fields with generalized tensor parameters, to accurately and efficiently analyze such objects is quite a challenge. Among numerous numerical methods, the method of moments (MoM) solution of the volume integral equation (VIE) [5], [6], in which the object is replaced by the equivalent volume currents according to the principle of volume equivalence, is one of top choices to analyze the general inhomogeneous bi-anisotropic objects. In [7], an integral equation based scheme was presented to analyze scattering from inhomogeneous bodies with anisotropic EM properties. An adaptive integral method was used to solve the EM scattering of inhomogeneous bi-anisotropic objects [8]. A generalized VIE method was formulated for arbitrarily shaped complex objects with inhomogeneous bi-isotropy [9], where the three-dimensional solenoidal function was incorporated as the basis function defined on each tetrahedron. In [10], a stable VIE formulation expanded with piecewise constant basis functions for extremely anisotropic materials was reported. It was concluded that when the scatterer is extremely anisotropic, the behavior of the VIE formulation based on the equivalent currents is more stable than that based on fluxes or fields. However, this conclusion is tenable only for the uniaxial anisotropic materials. Reference [11] proposed a new generalized volume-surface integral equation to analyze the EM scattering from composite objects comprised of both conductors and inhomogeneous bi-isotropic materials.

The associate editor coordinating the review of this manuscript and approving it for publication was Jenny Mahoney.

There are also some other novel articles contributing to VIE such as [12]–[14], about parallelization and preconditioner techniques.

The emphasis of this paper is to apply the efficient multilevel fast multipole algorithm (MLFMA) to the solution of VIE for arbitrary inhomogeneous bi-anisotropic materials. The classical MoM suffers from a large computational complexity which is on the order of N^2 due to the fully populated system matrices, where N is the number of unknowns. For a dielectric object computing by VIE, because of the dense volumetric discretization, N is bulky, leading to a large computational cost, even if for small electric size. Especially for the object involving bi-anisotropic material, compared with the common dielectric material for which the unknown coefficients are only needed to express the equivalent electric currents, the number of unknowns will be doubled since the unknown coefficients are needed to express both the electric and the magnetic currents simultaneously. It urgently calls for fast solvers such as the MLFMA. Based on the addition theorem of Green's function and diagonalization of the translation operator, the MLFMA drastically reduces the overall computational complexity to $O(N \log N)$ through three processes: aggregation, translation, and disaggregation accompanied with interpolation/anterpolation between levels [6]. In addition, the conventional MLFMA can be further improved by using the spherical harmonics expansion (SE). This SE-based MLFMA (denoted by SE-MLFMA) was first proposed in [15] to solve the surface integral equation (SIE) with dyadic representations, and then improved by using the mixed-potential representation of SIE [16]. The main idea of SE-MLFMA is briefly stated as follows [20]: In the implementation of conventional MLFMA, to enhance the computing efficiency, the so-called radiation patterns (RPs) of the basis functions which are the k-space samples over the Ewald sphere, should be computed and stored in advance. Because the quadrature sampling rate is determined by the bandwidth of the diagonalized translation matrix at the finest level, the RPs are oversampled, resulting in a significant amount of redundant memory usage. Utilizing the orthonormality, the RPs can be expanded as a series of the spherical harmonics. The expansion coefficients (ECs) instead of the RPs can be computed and stored, which will significantly reduce the memory requirement. Moreover, in the SE-MLFMA, both the aggregation of the outgoing waves and the disaggregation of the incoming waves at the finest level can also be executed in a faster way by summation of the spherical harmonics instead of the integrations in k-space. Therefore, the SE-MLFMA is even faster than the conventional one. However, due to the presence of bi-anisotropy, it is really not easy to apply the SE-MLFMA to such problems.

The goal of this paper is to implement the SE-MLFMA for general-purpose EM computation that can handle all kinds of material objects such as arbitrarily inhomogeneous anisotropy, bi-anisotropy, chirality, ferromagnetism, and isotropy. In Section II, it is shown in detail that how to yield the mixed-potential VIE for the inhomogeneous bi-anisotropy with general tensor parameters, while the classical MoM based on the Galerkin's testing with Schaubert-Wilton-Glisson (SWG) basis functions [17] is applied to convert the VIE into a matrix equation. In Section III, the MLFMA based on the integral strategy of tetrahedron-to-tetrahedron scheme is applied to solve the matrix equation, while how to use the SE to improve the conventional MFLMA to accelerate the iterative solution without sacrificing the solution accuracy is described subsequently. Some typical numerical results are shown in Section IV to demonstrate the accuracy and efficiency of the proposed method.

II. THEORY AND FORMULATIONS

A. DERIVATION OF VIE FOR COMPOSITE BI-ANISOTROPIC OBJECTS

Consider an object occupying a region V involving inhomogeneous materials which may be isotropic, bi-isotropic, anisotropic, or bi-anisotropic. It is assumed that this object is suspended in free space and illuminated by an incident plane EM wave $(\vec{E}^i, \vec{H}^i)$, and radiates the scattered field $(\vec{E}^s, \vec{H}^s)$. The coupled medium constitutive relationships for inhomogeneous bi-anisotropy between the electric flux density $\vec{D}$, magnetic flux density $\vec{B}$ and the electric field $\vec{E}$, magnetic field $\vec{H}$ are written as

$$\begin{bmatrix} \vec{E} \\ \vec{H} \end{bmatrix} = \begin{bmatrix} \bar{\bar{\varepsilon}} & \bar{\bar{\xi}} \\ \bar{\bar{\zeta}} & \bar{\bar{\mu}} \end{bmatrix}^{-1} \begin{bmatrix} \vec{D} \\ \vec{B} \end{bmatrix} = \begin{bmatrix} \bar{\bar{\alpha}}_{11} & \bar{\bar{\alpha}}_{12} \\ \bar{\bar{\alpha}}_{21} & \bar{\bar{\alpha}}_{22} \end{bmatrix} \begin{bmatrix} \vec{D} \\ \vec{B} \end{bmatrix} \tag{1}$$

where all of the parameters, permittivity $\bar{\bar{\varepsilon}}$, permeability $\bar{\bar{\mu}}$, and bi-anisotropic parameters $\bar{\bar{\xi}}$ and $\bar{\bar{\zeta}}$, are spatial tensors.

In the region V, the volume integral equation (VIE) is written as

$$\left(\vec{E}, \vec{H}\right) - \left(\vec{E}^s, \vec{H}^s\right) = \left(\vec{E}^i, \vec{H}^i\right) \tag{2}$$

Since the total EM field $(\vec{E}, \vec{H})$ is a superposition of incident and scattered fields, from the two curl equations of Maxwell's equations, the following equations

$$\begin{cases} \nabla \times \vec{E}^s = -j\omega\mu_0 \vec{H}^s - j\omega \left(\bar{\bar{\mu}} - \mu_0 \bar{\bar{I}}\right) \cdot \vec{H} - j\omega \bar{\bar{\zeta}} \cdot \vec{E} \\ \nabla \times \vec{H}^s = j\omega\varepsilon_0 \vec{E}^s + j\omega \left(\bar{\bar{\varepsilon}} - \varepsilon_0 \bar{\bar{I}}\right) \cdot \vec{E} + j\omega \bar{\bar{\xi}} \cdot \vec{H} \end{cases} \tag{3}$$

can be obtained, where $j = \sqrt{-1}$ with the time-harmonic factor $e^{j\omega t}$, ω is the angular frequency, ε_0 and μ_0 are the permittivity and permeability of free space, $\bar{\bar{I}}$ denotes the identity tensor, respectively. According to the principle of volume equivalence, $(\vec{E}^s, \vec{H}^s)$ can be seen as production by both the equivalent volume electric and magnetic currents $\vec{J}$ and $\vec{M}$ in free space. By comparing (3) with the Maxwell's equations and substituting (1), $\vec{J}$ and $\vec{M}$ for bi-anisotropy are derived by

$$\begin{aligned} \begin{bmatrix} \vec{J} \\ \vec{M} \end{bmatrix} &= j\omega \begin{bmatrix} \bar{\bar{I}} - \varepsilon_0 \bar{\bar{\alpha}}_{11} & -\varepsilon_0 \bar{\bar{\alpha}}_{12} \\ -\mu_0 \bar{\bar{\alpha}}_{21} & \bar{\bar{I}} - \mu_0 \bar{\bar{\alpha}}_{22} \end{bmatrix} \begin{bmatrix} \vec{D} \\ \vec{B} \end{bmatrix} \\ &= j\omega \begin{bmatrix} \bar{\bar{\beta}}_{11} & \bar{\bar{\beta}}_{12} \\ \bar{\bar{\beta}}_{21} & \bar{\bar{\beta}}_{22} \end{bmatrix} \begin{bmatrix} \vec{D} \\ \vec{B} \end{bmatrix} \end{aligned} \tag{4}$$

Parenthetically, $(\vec{E}^s, \vec{H}^s)$ can be carried out using the mixed-potential form [7] or the dyadic form [9], while the former one results in a brief representation and is convenient to combine with the MLFMA. Therefore, in the implementation, $(\vec{E}^s, \vec{H}^s)$ is cast in terms of mixed auxiliary potentials as

$$\begin{cases} \vec{E}^s = -j\omega\vec{A}_J - \nabla\varphi_J - \dfrac{1}{\varepsilon_0}\nabla\times\vec{A}_M \\ \vec{H}^s = -j\omega\vec{A}_M - \nabla\varphi_M + \dfrac{1}{\mu_0}\nabla\times\vec{A}_J \end{cases} \tag{5}$$

with

$$\begin{cases} \vec{A}_J = \mu_0\int_V \vec{J}\left(\vec{r}'\right) G\left(\vec{r},\vec{r}'\right) dV' \\ \varphi_J = \dfrac{j}{\omega\varepsilon_0}\displaystyle\int_V \nabla'\cdot\vec{J}\left(\vec{r}'\right) G\left(\vec{r},\vec{r}'\right) dV' \end{cases} \tag{6}$$

where $\vec{r}$ and $\vec{r}'$ are the observation and source points, respectively, while $\vec{A}_M$ and φ_M can be found using the duality. Besides, the Green's function of free space is expressed as

$$G\left(\vec{r},\vec{r}'\right) = \frac{e^{-jk|\vec{r}-\vec{r}'|}}{4\pi\,|\vec{r}-\vec{r}'|} \tag{7}$$

with the wavenumber $k = \omega\sqrt{\mu_0\varepsilon_0}$.

B. MOM SOLUTION USING SWG BASIS FUNCTION

Using the MoM, the VIE is converted into a matrix equation. In the implementation, the divergence conforming SWG basis function [17] is used to respectively disperse $\vec{D}$ and $\vec{B}$ in V as

$$\vec{D} = \frac{1}{j\omega}\sum_{i=1}^{N} I_i^D\vec{f}_i \quad \vec{B} = \frac{\eta_0}{j\omega}\sum_{i=1}^{N} I_i^B\vec{f}_i \tag{8}$$

Dispersing $\vec{D}$ and $\vec{B}$ instead of $\vec{J}$ and $\vec{M}$ can hold the continuity of the normal components which are consistent with the boundary condition for dielectric interfaces. In (8), N is the number of SWG basis functions $\vec{f}_i$, while the total number of unknowns is $2N$. I_i^D and I_i^B are the corresponding unknown coefficients, respectively. It is assumed that $\bar{\bar{\varepsilon}}$, $\bar{\bar{\mu}}$, $\bar{\bar{\xi}}$ and $\bar{\bar{\zeta}}$ are approximately constant tensors within each tetrahedron, which is a generalization of that presented in [17]. As a consequence, the 6×6 matrices $[\bar{\bar{\alpha}}]$ and $[\bar{\bar{\beta}}]$ defined in (1) and (4) over a single tetrahedron are also considered as constant matrices. Substituting (8) into (2)-(6) as well as using Galerkin's testing results in an impedance matrix equation of the MoM, which can succinctly be represented as

$$\begin{bmatrix} Z^{DD} & Z^{DB} \\ Z^{BD} & Z^{BB} \end{bmatrix} \begin{Bmatrix} I^D \\ I^B \end{Bmatrix} = \begin{Bmatrix} b^D \\ b^B \end{Bmatrix} \tag{9}$$

where $\{b^D\}$ and $\{b^B\}$ are the excitation vectors. The matrix entries are given by

$$\begin{cases} Z^{DD} = W\left(\bar{\bar{\alpha}}_{11}, \bar{\bar{\beta}}_{11}, \bar{\bar{\beta}}_{21}, \varepsilon_0, \mu_0\right) \\ Z^{DB} = W\left(\bar{\bar{\alpha}}_{12}, \bar{\bar{\beta}}_{12}, \bar{\bar{\beta}}_{21}, \varepsilon_0, \mu_0\right) \\ Z^{BD} = W\left(\bar{\bar{\alpha}}_{21}, \bar{\bar{\beta}}_{21}, -\bar{\bar{\beta}}_{11}, \mu_0, \varepsilon_0\right) \\ Z^{BB} = W\left(\bar{\bar{\alpha}}_{22}, \bar{\bar{\beta}}_{22}, -\bar{\bar{\beta}}_{12}, \mu_0, \varepsilon_0\right) \end{cases} \tag{10}$$

with the entry in the jth row and ith column

$$\begin{aligned} &W_{ji}\left(\bar{\bar{\alpha}}_{x_1y}, \bar{\bar{\beta}}_{x_1y}, \bar{\bar{\beta}}_{x_2y}, \chi, \gamma\right) \\ &= \frac{1}{j\omega}\int_{V_j}\vec{f}_j\cdot\bar{\bar{\alpha}}_{x_1y}\cdot\vec{f}_i dV + j\omega\gamma\int_{V_j}\vec{f}_j\cdot\int_{V_i}\bar{\bar{\beta}}_{x_1y} \\ &\quad\cdot\vec{f}_i G\left(\vec{r},\vec{r}'\right) dV'dV \\ &\quad + \frac{j}{\omega\chi}\int_{V_j}\vec{f}_j\cdot\nabla\int_{V_i}\nabla'\cdot\left(\bar{\bar{\beta}}_{x_1y}\cdot\vec{f}_i\right) G\left(\vec{r},\vec{r}'\right) dV'dV \\ &\quad + \int_{V_j}\vec{f}_j\cdot\nabla\times\int_{V_i}\bar{\bar{\beta}}_{x_2y}\cdot\vec{f}_i G\left(\vec{r},\vec{r}'\right) dV'dV \end{aligned} \tag{11}$$

where the subscripts $x_1, x_2, y = 1$ or 2 and $x_1 + x_2 \equiv 3$.

The ith SWG basis function relative to the tetrahedron T_n of volume v_n is defined over a face of area a_i shared by two adjacent tetrahedrons as

$$\vec{f}_i\left(\vec{r}'\right) = \mathrm{sgn}\left(n_i\right)\frac{a_i}{3v_n}\left(\vec{r}' - \vec{r}_n^i\right) \quad \forall\vec{r}' \in T_n \tag{12}$$

where $\mathrm{sgn}(n_i) = 1$ or -1 means that the current flowing direction of the ith basis function is outward or inward relative to T_n, and $\vec{r}_n^i$ is the free vertex of the ith basis function to T_n [17]. Particularly, at the boundary of object, since the flux density is not necessarily zero, a "half" SWG basis function is defined over the interior tetrahedron.

To optimize the performance, the algorithm should be designed to maximally reduce the computational time. For this purpose, in this paper, the interactions between testing and basis functions are generally computed in a tetrahedron-to-tetrahedron manner, rather than using the direct testing-to-basis functions one. From the following analysis in Section III, it can be found that this manner also causes a lower memory requirement to store the RPs or ECs. Then in any case, each double volume integral in (11) consists of up to four sub-integrals of the same type, which represent the mutual interactions between tetrahedrons involved in the testing and basis functions. The final result of (11) can be efficiently obtained by adding the contributions of all related tetrahedron-to-tetrahedron integrals to the testing-to-basis entry. Therefore, in the following, only the sub-integral between two "positive" tetrahedrons is considered, while other three ones can be obtained by simply changing the sign. For convenience, tetrahedrons T_m and T_n of volumes v_m and v_n are assumed as the two "positive" tetrahedrons involving the jth testing and ith basis functions, respectively. Thus, the matrix entries in (11) rely on the evaluation of four kinds of integrations as

$$\begin{aligned} I_1 &= \int_{T_m}\vec{f}_j\left(\vec{r}\right)\cdot\bar{\bar{\alpha}}_{x_1y}\cdot\vec{f}_i\left(\vec{r}\right) dV \\ I_2 &= \frac{a_j a_i}{9v_m v_n}\int_{T_m}\left(\vec{r} - \vec{r}_m^j\right)\cdot\bar{\bar{\beta}}_{x_1y} \\ &\quad\cdot\int_{T_n}\left(\vec{r}' - \vec{r}_n^i\right) G\left(\vec{r},\vec{r}'\right) dV'dV \end{aligned}$$

$$I_3 = \frac{a_j a_i}{9 v_m v_n} \int_{T_m} \left(\vec{r} - \vec{r}_m^{\,j}\right) \cdot \nabla \int_{T_n} \nabla' \cdot \left[\bar{\bar{\beta}}_{x_1 y} \cdot \left(\vec{r}' - \vec{r}_n^{\,i}\right)\right] G\left(\vec{r}, \vec{r}'\right) dV' dV$$

$$I_4 = \frac{a_j a_i}{9 v_m v_n} \int_{T_m} \left(\vec{r} - \vec{r}_m^{\,j}\right) \cdot \nabla \times \int_{T_n} \bar{\bar{\beta}}_{x_2 y} \cdot \left(\vec{r}' - \vec{r}_n^{\,i}\right) G\left(\vec{r}, \vec{r}'\right) dV' dV \tag{13}$$

Apparently, I_1 can be evaluated analytically or numerically without any singularity. I_2 has singularity of order one when $\vec{r} \to \vec{r}'$, which can be expediently handled using either the singularity extraction method [18] or Duffy transform [19]. According to $\nabla \times \vec{r} \equiv 0$ and the Gauss theorem, I_4 can be transformed into a surface-volume integration with also singularity of order one during $\vec{r} \to \vec{r}'$. For the evaluation of I_3, it is divided into two parts as

$$I_3 = \frac{a_j a_i}{9 v_m v_n} \int_{T_m} \nabla \cdot \left\{ \left(\vec{r} - \vec{r}_m^{\,j}\right) \int_{T_n} \nabla' \cdot \left[\bar{\bar{\beta}}_{x_1 y} \cdot \left(\vec{r}' - \vec{r}_n^{\,i}\right)\right] G\left(\vec{r}, \vec{r}'\right) dV' \right\} dV - \frac{a_j a_i}{9 v_m v_n} \int_{T_m} \nabla \cdot \left(\vec{r} - \vec{r}_m^{\,j}\right) \int_{T_n} \nabla' \cdot \left[\bar{\bar{\beta}}_{x_1 y} \cdot \left(\vec{r}' - \vec{r}_n^{\,i}\right)\right] G\left(\vec{r}, \vec{r}'\right) dV' dV \tag{14}$$

The inner integration involving the divergence calculation in (14) can be calculated as

$$\int_{T_n} \nabla' \cdot \left[\bar{\bar{\beta}}_{x_1 y} \cdot \left(\vec{r}' - \vec{r}_n^{\,i}\right)\right] G\left(\vec{r}, \vec{r}'\right) dV' = \mathrm{Tr}\left(\bar{\bar{\beta}}_{x_1 y}\right) \int_{T_n} G\left(\vec{r}, \vec{r}'\right) dV' - \oint_{\partial T_n} \hat{n}_{\partial T_n} \cdot \left[\bar{\bar{\beta}}_{x_1 y} \cdot \left(\vec{r}' - \vec{r}_n^{\,i}\right)\right] G\left(\vec{r}, \vec{r}'\right) dS' \tag{15}$$

where $\mathrm{Tr}\bar{\bar{\beta}}_{x_1 y}$) denotes the trace of $\bar{\bar{\beta}}_{x_1 y}$, ∂T_n denotes the four triangular faces bounding the tetrahedron T_n, and $\hat{n}_{\partial T_n}$ is the outward normal vector to ∂T_n [7]. For the first item of the right-hand side (RHS) in (14), according to the Gauss theorem, the outer volume-integration can be transformed into surface-integration as

$$\begin{aligned} &\int_{T_m} \nabla \cdot \left\{ \left(\vec{r} - \vec{r}_m^{\,j}\right) \int_{T_n} \nabla' \cdot \left[\bar{\bar{\beta}}_{x_1 y} \cdot \left(\vec{r}' - \vec{r}_n^{\,i}\right)\right] G\left(\vec{r}, \vec{r}'\right) dV' \right\} dV \\ &= \oint_{\partial T_m} \hat{n}_{\partial T_m} \cdot \left(\vec{r} - \vec{r}_m^{\,j}\right) \int_{T_n} \nabla' \cdot \left[\bar{\bar{\beta}}_{x_1 y} \cdot \left(\vec{r}' - \vec{r}_n^{\,i}\right)\right] G\left(\vec{r}, \vec{r}'\right) dV' dS \\ &= \frac{3 v_m}{a_j} \delta_j \int_{S_m^j} \int_{T_n} \nabla' \cdot \left[\bar{\bar{\beta}}_{x_1 y} \cdot \left(\vec{r}' - \vec{r}_n^{\,i}\right)\right] G\left(\vec{r}, \vec{r}'\right) dV' dS \end{aligned} \tag{16}$$

where $\delta_j = 0$ or 1 when the jth testing function is "full" or "half". The above derivation is based on this fact: only when $\vec{r}$ locates in the opposite face (denoted by S_m^j) of the free vertex $\vec{r}_m^{\,j}$, does $\hat{n}_{\partial T_m} \cdot (\vec{r} - \vec{r}_m^{\,j})$ not equal to 0. Further, if the jth testing function is "full" which is defined on two adjacent tetrahedrons, the two integrations over these two tetrahedrons will have the same value while opposite sign, i.e., $\delta_j = 0$. On the contrary, for the jth "half" testing function associated with a single tetrahedron, $\delta_j = 1$. With (14)-(16), the singularity of I_3 is reduced to order one, which can be evaluated numerically.

III. MLFMA IMPLIMENTATION

During the implementation of MLFMA, the MoM matrix is decomposed into two parts as $Z_{\text{near}} + Z_{\text{far}}$, where Z_{near} and Z_{far} are the impedance matrices representing the interactions between the testing and basis functions in the near and far groups, respectively. Only Z_{near} is computed using the classical MoM and stored explicitly, while the computation of matrix-vector product (MVP) involving Z_{far} is implicit. Besides, since Z_{far} denotes the far-group interaction, I_2, I_3 and I_4 in (13) will be included in Z_{far}, while I_1 representing the "self" term contribution is eliminated.

A. DERIVATION OF THE CONVENTIONAL MLFMA

In the setup of MLFMA, the basis functions need to be grouped according to the octree. In this paper, since the interactions between SWG testing and basis functions are computed in a tetrahedron-to-tetrahedron manner, the grouping scheme is based on the tetrahedrons, rather than the commonly used face-based one [6]. That is to say, the index of the leaf box to which a given tetrahedron belongs is determined by comparing the center coordinate of the leaf box with that of the barycenter of tetrahedron. If T_m and T_n are grouped into the m'th and n'th leaf boxes of the center coordinates $\vec{r}_{m'}$ and $\vec{r}_{n'}$, respectively, via the addition theorem, the Green's function will be rewritten as

$$G\left(\vec{r}, \vec{r}'\right) = \oint e^{-j\vec{k}\cdot(\vec{r} - \vec{r}_{m'})} T_L e^{-j\vec{k}\cdot(\vec{r}_{n'} - \vec{r}')} d^2\hat{k} \tag{17}$$

with the translation operator T_L[6].

For convenience, beforehand, we define

$$\begin{cases} \tilde{S}_\psi\left(\vec{k}\right) = \int_{T_\psi} e^{-j\vec{k}\cdot\left(\vec{r}_{\psi'} - \vec{r}'\right)} dV' \\ \tilde{\bar{V}}_\psi\left(\vec{k}\right) = \int_{T_\psi} \vec{r}' e^{-j\vec{k}\cdot\left(\vec{r}_{\psi'} - \vec{r}'\right)} dV' \\ \tilde{F}_\psi^o\left(\vec{k}\right) = \int_{S_\psi^o} e^{-j\vec{k}\cdot\left(\vec{r}_{\psi'} - \vec{r}'\right)} dS' \\ \tilde{\bar{Q}}_n^o\left(\vec{k}\right) = \int_{S_n^o} \vec{r}' e^{-j\vec{k}\cdot(\vec{r}_{n'} - \vec{r}')} dS' \end{cases} \quad \psi = m, n \tag{18}$$

and

$$\tilde{\bar{G}}_\psi^\Lambda\left(\vec{k}\right) = \frac{a_\Lambda}{3 v_\psi} \left[\tilde{\bar{V}}_\psi\left(\vec{k}\right) - \vec{r}_\psi^{\,\Lambda} \tilde{S}_\psi\left(\vec{k}\right)\right] \quad \Lambda = i, j \tag{19}$$

With (17)-(19), I_2 and I_3 respectively become

$$I_2 = \oint \left[\tilde{\bar{G}}_m^j\left(\vec{k}\right)\right]^* \cdot T_L \bar{\bar{\beta}}_{x_1 y} \cdot \tilde{\bar{G}}_n^i\left(\vec{k}\right) d^2\hat{k} \tag{20}$$

and

$$I_3 = \oint \left\{ \begin{array}{l} \left[\delta_j \tilde{F}_m^j \left(\vec{k} \right) - \frac{a_j}{v_m} \tilde{S}_m \left(\vec{k} \right) \right]^* T_L \\ \frac{a_i}{3v_n} \left\{ \begin{array}{l} \mathrm{Tr} \left(\bar{\bar{\beta}}_{x_1 y} \right) \tilde{S}_n \left(\vec{k} \right) - \\ \sum_{o=1}^{4} \left\{ \left(\bar{\bar{\beta}}_{x_1 y}^T \cdot \hat{n}_{S_n^o} \right) \cdot \left[\tilde{\vec{Q}}_n^o \left(\vec{k} \right) - \vec{r}_i^n \tilde{F}_n^o \left(\vec{k} \right) \right] \right\} \end{array} \right\} \end{array} \right\} \times d^2 \hat{k} \quad (21)$$

where "$*$" denotes the complex conjugate, $\bar{\bar{\beta}}_{x_1 y}^T$ means the transpose of $\bar{\bar{\beta}}_{x_1 y}$, S_n^o $(o = 1, 2, 3, 4)$ denotes the set of four faces belonging to the tetrahedron T_n, respectively. For I_4, because the singularity problem is nonexistent in the far-group interaction, we can safely choose the expression form of (13). According to $\nabla \times \left(\bar{\bar{\beta}}_{x_2 y} \cdot \vec{r}' \right) \equiv 0$ and the addition theorem, I_4 is transformed to

$$\begin{aligned} I_4 &= -\frac{a_j a_i}{9 v_m v_n} \int_{T_m} \left(\vec{r} - \vec{r}_m^j \right) \cdot \int_{T_n} \left[\bar{\bar{\beta}}_{x_2 y} \cdot \left(\vec{r}' vec r_n^i \right) \right] \\ &\quad \times \nabla G \left(\vec{r}, \vec{r}' \right) dV' dV \\ &= j \oint \left[\tilde{\vec{G}}_m^j \left(\vec{k} \right) \right]^* \cdot T_L \left\{ \left[\bar{\bar{\beta}}_{x_2 y} \cdot \tilde{\vec{G}}_n^i \left(\vec{k} \right) \right] \times \vec{k} \right\} d^2 \hat{k} \end{aligned} \quad (22)$$

Following by a series of elaborate transformations, the "positive-to-positive" part of the Z_{far} entry is written as In (23), as shown at the top of the next page, the first and the second parts of RHS are the vector and the scalar corresponding computations, respectively. It is seen that the scalar $\tilde{S}_\Psi$ and vector $\tilde{\vec{V}}_\Psi$ involving the volume integration, as well as the scalar $\tilde{F}_\Psi$ and vector $\tilde{\vec{Q}}_n$ involving the surface integration, contain all information needed by the aggregation process in the conventional MLFMA, which means that they can be regarded as the RPs defined for a given tetrahedron but not for a SWG basis function as shown in [7]. Besides, contribute to the symmetry of the tetrahedrons RPs, complex conjugates of $\tilde{S}_\Psi$, $\tilde{\vec{V}}_\Psi$ and $\tilde{F}_\Psi$ are also reused as the receiving patterns in the disaggregation process.

In addition, during the implementation, because the parameters χ and γ involving in the evaluation of $[Z^{DD}]$ and $[Z^{DB}]$ in (10) are different from that of $[Z^{BD}]$ and $[Z^{BB}]$, the single MVP has to be accomplished through two individual MLFMA processes. In other words, one MVP in (9) should be divided into two individual MLFMA implementations: $[Z^{DD}]\{I^D\} + [Z^{DB}]\{I^B\}$ and $[Z^{BD}]\{I^D\} + [Z^{BB}]\{I^B\}$. Since these two processes are irrelevant, they can be independently carried out. If we elaborately merge χ and γ into the aggregation process as shown in (23), the two individual MLFMA processes will share an identical disaggregation process, which can greatly simplify the work of programmatic implementation.

B. IMPROVING CONVENTIONAL MLFMA USING SE

In the conventional MLFMA, during the precomputation and storage of the tetrahedrons RPs (18), the number of quadrature points is $2(L+1)^2$, where L is the order of multipole expansion [6]. In the SE-MLFMA, these RPs are expressed as a series of the spherical harmonics as

$$\left\{ \begin{array}{l} \tilde{S}_\psi \left(\hat{k} \right) = \sum_{p=0}^{P} \sum_{q=-p}^{p} S_{pq}^\psi Y_{pq} \left(\hat{k} \right) \\ \tilde{\vec{V}}_\psi \left(\hat{k} \right) = \sum_{p=0}^{P} \sum_{q=-p}^{p} \vec{V}_{pq}^\psi Y_{pq} \left(\hat{k} \right) \\ \tilde{F}_\psi \left(\hat{k} \right) = \sum_{p=0}^{P} \sum_{q=-p}^{p} F_{pq}^\psi Y_{pq} \left(\hat{k} \right) \\ \tilde{\vec{Q}}_n \left(\hat{k} \right) = \sum_{p=0}^{P} \sum_{q=-p}^{p} \vec{Q}_{pq}^n Y_{pq} \left(\hat{k} \right) \end{array} \right.$$

$$\times \left\{ \begin{array}{l} S_{pq}^\psi = \oint \tilde{S}_\psi \left(\hat{k} \right) Y_{pq}^* \left(\hat{k} \right) d^2 \hat{k} \\ \vec{V}_{pq}^\psi = \oint \tilde{\vec{V}}_\psi \left(\hat{k} \right) Y_{pq}^* \left(\hat{k} \right) d^2 \hat{k} \\ F_{pq}^\psi = \oint \tilde{F}_\psi^o \left(\hat{k} \right) Y_{pq}^* \left(\hat{k} \right) d^2 \hat{k} \\ \vec{Q}_{pq}^n = \oint \tilde{\vec{Q}}_n^o \left(\hat{k} \right) Y_{pq}^* \left(\hat{k} \right) d^2 \hat{k} \end{array} \right. \quad (24)$$

where Y_{pq} is the orthornomalized spherical harmonics [20], and P is the degree of SE. The ECs, instead of RPs, are computed and stored in the setup of the SE-MLFMA. The error from the introduced SE is controllable with the choose of P, which is typically dependent on the spectral content of the tetrahedrons RPs as given by (18). For the purpose of saving memory, the number of coefficients must be considerably smaller than that of quadrature points used to numerically compute the integrations in (18). In other words, P is must smaller than L. In [21], it is found that under the spherical coordinate, the spherical harmonics representing the outgoing waves of a leaf box are rapidly decaying when $P \geq L/2$ in an appropriately designed MLFMA. Moreover, P can be one less if the SE is performed in the Cartesian coordinate instead of in the spherical one [15], leading to a much lower memory requirement for a relatively small P. Actually, under the general size of leaf box in a sophisticated MLFMA, L is usually fixed from 5 to 7 accompanied with P from 2 to 3. Since the expression of RPs in (18) is under Cartesian coordinate, we may choose $P = L/2 - 1$ in our implementation, while $P = 1$ is not recommended in practice. The detail analysis about the value of P to the calculation error can be found in [21].

The following will show how to elaborately use the orthonormality of spherical harmonics to execute the aggregation and disaggregation processes at the finest level in a faster way. If we assume that $\tilde{\vec{V}}_{n'}$ and $\tilde{S}_{n'}$ are respectively the summation of the vector and scalar outgoing waves for all tetrahedrons belonging to the n'th leaf box, they will be

$$
\begin{aligned}
&W_{ji}^{++}\left(\bar{\bar{\beta}}_{x_1y},\bar{\bar{\beta}}_{x_2y},\chi,\gamma\right)\\
&=j\oint\left\{\underbrace{\left[\tilde{\bar{G}}_m^j\left(\vec{k}\right)\right]^*}_{disaggregation}\cdot T_L\underbrace{\left\{\begin{array}{l}\omega\gamma\bar{\bar{\beta}}_{x_1y}\cdot\tilde{\bar{G}}_n^i\left(\vec{k}\right)\\+\left[\bar{\bar{\beta}}_{x_2y}\cdot\tilde{\bar{G}}_n^i\left(\vec{k}\right)\right]\times\vec{k}\end{array}\right\}}_{aggregation}\right\}d^2\hat{k}\\
&+j\oint\left\{\begin{array}{l}\underbrace{\left[\delta_j\tilde{F}_m^j\left(\vec{k}\right)-\dfrac{a_j}{v_m}\tilde{S}_m\left(\vec{k}\right)\right]^*}_{disaggregation}T_L\\\underbrace{\dfrac{a_i}{3\omega\chi v_n}\left\{\begin{array}{l}Tr\left(\bar{\bar{\beta}}_{x_1y}\right)\tilde{S}_n\left(\vec{k}\right)\\-\sum\limits_{o=1}^{4}\left\{\left(\bar{\bar{\beta}}_{x_1y}^T\cdot\hat{n}_{S_n^o}\right)\cdot\left[\tilde{\bar{Q}}_n^o\left(\vec{k}\right)-\vec{r}_i^n\tilde{F}_n^o\left(\vec{k}\right)\right]\right\}\end{array}\right\}}_{aggregation}\end{array}\right\}d^2\hat{k}
\end{aligned}
\tag{23}
$$

carried out according to

$$
\left\{\begin{array}{l}\tilde{\bar{\mathcal{V}}}_{n'}\left(\vec{k}\right)=j\omega\gamma\sum\limits_{p=0}^{P}\sum\limits_{q=-p}^{p}\vec{\mathcal{V}}_{pq}^{n'}\left(\bar{\bar{\beta}}_{x_1y}\right)Y_{pq}\left(\hat{k}\right)\\\qquad\qquad+j\sum\limits_{p=0}^{P}\sum\limits_{q=-p}^{p}\vec{\mathcal{V}}_{pq}^{n'}\left(\bar{\bar{\beta}}_{x_2y}\right)Y_{pq}\left(\hat{k}\right)\times\vec{k}\\\tilde{\mathcal{S}}_{n'}\left(\vec{k}\right)=\dfrac{j}{\omega\chi}\sum\limits_{p=0}^{P}\sum\limits_{q=-p}^{p}\mathcal{S}_{pq}^{n'}Y_{pq}\left(\hat{k}\right)\end{array}\right.
\tag{25}
$$

with

$$
\left\{\begin{array}{l}\vec{\mathcal{V}}_{pq}^{n'}\left(\bar{\bar{\beta}}\right)=\sum\limits_{n}^{N'}\bar{\bar{\beta}}\cdot\sum\limits_{i}^{X_n}sgn\left(n_i\right)\dfrac{a_i}{3v_n}\left(\tilde{\vec{V}}_{pq}^{n}-\vec{r}_n^i\tilde{S}_{pq}^{n}\right)I_i\\\mathcal{S}_{pq}^{n'}=\sum\limits_{n}^{N'}\sum\limits_{i}^{X_n}sgn\left(n_i\right)\dfrac{a_i}{3v_n}\\\qquad\times\left[\begin{array}{l}Tr\left(\bar{\bar{\beta}}_{x_1y}\right)\tilde{S}_{pq}^{n}-\\\sum\limits_{o=1}^{4}\left(\bar{\bar{\beta}}_{x_1y}^T\cdot\hat{n}_{S_n^o}\right)\cdot\left(\tilde{\bar{Q}}_{pq}^{n}-\vec{r}_i^n\tilde{F}_{pq}^{n}\right)\end{array}\right]I_i\end{array}\right.
\tag{26}
$$

where N' denotes the set of all the tetrahedrons belonging to the n'th leaf box, and X_n stands for the four indexes of SWG basis functions involving in the tetrahedron T_n. The translations from outgoing to incoming waves as well as the aggregations and disaggregations between levels accompanied with interpolation and anterpolation are performed in the same manner as those in the conventional MLFMA [6]. However, when all incoming waves are collected in a certain group at the finest level, the orthonormality of spherical harmonics can also be utilized. If $\tilde{\bar{\mathcal{Q}}}_{m'}$ and $\tilde{\mathcal{P}}_{m'}$ are assumed the vector and scalar total incoming waves collected into the center of m'th leaf box respectively, the vector and the scalar expansion coefficients for this box will be

$$
\left\{\begin{array}{l}\vec{\mathcal{Q}}_{pq}^{m'}=\oint\tilde{\bar{\mathcal{Q}}}_{m'}\left(\vec{k}\right)Y_{pq}^*\left(\hat{k}\right)d^2\hat{k}\\\mathcal{Q}_{pq}^{m'}=\oint\tilde{\mathcal{P}}_{m'}\left(\vec{k}\right)Y_{pq}^*\left(\hat{k}\right)d^2\hat{k}\end{array}\right.
\tag{27}
$$

The disaggregation process in the m'th leaf box is executed according to

$$
\begin{aligned}
b_j=&\sum_{m}^{m^+,m^-}sgn\left(m_j\right)\\
&\times\sum_{p=0}^{P}\sum_{q=-p}^{p}\left\{\begin{array}{l}\frac{a_j}{3v_m}\left(\tilde{\vec{V}}_{pq}^{m}-\vec{r}_m^j\tilde{S}_{pq}^{m}\right)^*\cdot\vec{\mathcal{Q}}_{pq}^{m'}\\+\left[\delta_j\left(\tilde{F}_{pq}^{m}\right)^*-\dfrac{a_j}{v_m}\left(\tilde{S}_{pq}^{m}\right)^*\right]\mathcal{P}_{pq}^{m'}\end{array}\right\}
\end{aligned}
\tag{28}
$$

while m^+ and m^- denote the two indexes of adjacent tetrahedrons on which the jth testing function is defined.

The proposed SE-MLFMA to solve the bi-anisotropic problems exhibits two advantages as follows. Firstly, it has a low memory requirement. In the conventional MLFMA, according to (18), we need to store a scalar and a vector components for each tetrahedron ($\tilde{S}_\Psi$ and $\tilde{\vec{V}}_\Psi$) and each triangular face ($\tilde{F}_\Psi$ and $\tilde{\bar{\mathcal{Q}}}_n$), respectively. If the integrations in (18) are evaluated using Gauss Legendre rule, with the symmetry of the k-space, the memory requirement in bytes to store the RPs of tetrahedrons is

$$
\mathrm{Mem}_{RP}=4\left(N_t+N\right)\left(L+1\right)^2c_2
\tag{29}
$$

where N_t and N are the numbers of tetrahedrons and triangular faces, respectively, and the constant c_2 is either 8 or 16 for a single precision or double precision. By contrast, in the SE-MLFMA, the ECs of spherical harmonics in (24) are stored instead of the RPs. Similar with the above description about storing RPs, S_{pq}^{Ψ} and $\vec{V}_{pq}^{\Psi}$ for each tetrahedron as well as F_{pq}^{Ψ} and $\vec{\mathcal{Q}}_{pq}^{\Psi}$ for each triangular face are stored, while the memory

requirement in bytes is

$$\mathrm{Mem}_{SE} = 2\,(N_t + N)\,(P+1)\,(P+2)\,c_2 \tag{30}$$

As stated above, in Cartesian coordinate, the SE degree$P$ is usually selected as $\max(2, L/2-1)$. Therefore, compared with (29), (30) shows a significant decrease in the memory requirement. Besides, we define a ratio R_M as

$$R_M = \frac{\mathrm{Mem}_{RP}}{\mathrm{Mem}_{SE}} = \frac{2\,(L+1)^2}{(P+1)\,(P+2)} \tag{31}$$

which depends on L and Ponly. Thus, (31) is suitable for all kinds of numerical experiments. For instance, when the leaf box size is 0.2λ (λ is the wavelength in free space), then $L = 5$ with $P = 2$ according to a moderate truncation order [6]. In this case, R_M is 6, which means that the memory requirement of storing RPs is 6 times of storing ECs. On the other hand, (29) and (30) are derived basing on the tetrahedron-to-tetrahedron scheme of integrations. If the commonly used face-to-face integral scheme is adopted during the implementation of conventional MLFMA [7]–[10], the memory requirement to store the components of RPs ($\tilde{\tilde{S}}_\Psi$ and $\tilde{\tilde{V}}_\Psi$) or ECs (S_{pq}^{Ψ} and $\vec{V}_{pq}^{\Psi}$) involving volume integrations will also be proportional to N rather than N_t. Since N is much larger than N_t, the memory requirement for the face-to-face scheme is much bigger than that for the tetrahedron-to-tetrahedron one.

Secondly, the proposed method is easy to be implemented without repeat transformations between different coordinates. In this paper, the VIE is expressed by the mixed-potential representation in Cartesian coordinate, which is solved using the SE-MLFMA under the same coordinate. However, if the VIE is expressed by the commonly used dyadic representation in spherical coordinate, additional operations will be required. Because P can be one less if the SE is performed for the Cartesian components instead of the spherical ones, storing the ECs obtained in Cartesian coordinate shows a lower memory requirement than that in spherical coordinate. Moreover, due to the truncations of the spherical components, the Gibb's phenomenon will arise if the integrations of the spherical harmonics are evaluated in spherical coordinate, while the Cartesian components are continuous without the above problem. Thus, executing the process of SE in Cartesian coordinate is essential. Consequently, if the dyadic representation of VIE is adopted in the spherical coordinate, in order to use a relatively small SE degree P as well as to avoid the Gibb's phenomenon, the spherical components of the RPs need to be first transformed to Cartesian ones for the SE procedure, which should be transformed back to the spherical coordinate for upward aggregation. Similar operation needs to be performed one more time during the disaggregation process at the finest level. These repeated transformations between different coordinates will increase the computation time. On the contrary, in our implementation, due to the mixed-potential representation of VIE, not only the SE procedure, but also the aggregation, translation, and disaggregation processes are all operated in the Cartesian coordinate, which totally eliminates the repeated transformations between different coordinates, leading to a faster implementation.

IV. NUMERICAL RESULTS

The radar cross section (RCS) results of several objects with anisotropic, bi-isotropic or bi-anisotropic material are calculated. The target relative residual error in the iterative solver is 0.001. Since VIE is a second-kind Fredholm integral equation, resulting in a well-conditioned impedance matrix, all examples can be converged in about dozen iterations. Unless otherwise stated, the leaf box size of the MLFMA is fixed to 0.2λ. All computations are carried out serially in single precision on a workstation with 2.4 GHz CPU and 384 GB RAM. During the comparison, the root-mean-square (RMS) error is used in the study, which is defined as

$$\mathrm{RMS} = \sqrt{\frac{1}{M}\sum_{i=1}^{M}\left|\sigma_i^{\mathrm{cal}} - \sigma_i^{\mathrm{Mie}}\right|^2} \tag{32}$$

where M is the number of observation angles, and σ_i^{cal} and σ_i^{Mie} denote the calculated and the Mie RCS results in the ith observation angle, respectively, measured in dB.

The first object is an inhomogeneous anisotropic spherical shell illuminated by a θ-polarized EM plane wave at frequency 140 MHz from $+z$-axis, while the observation range is $-180^\circ \leqslant \theta \leqslant 180^\circ$ in xzplane. The outer radius is 1 m, while the thickness of the shell is 0.055 m. An average mesh size of 0.06 m yields 10,593 tetrahedrons and 48,350 unknowns, respectively. The medium parameters are defined under the spherical coordinate as $\overline{\overline{\varepsilon}} = \mathrm{diag}(\varepsilon_r\varepsilon_0, \varepsilon_\theta\varepsilon_0, \varepsilon_\varphi\varepsilon_0)$, $\overline{\overline{\mu}} = \mathrm{diag}(\mu_r\mu_0, \mu_\theta\mu_0, \mu_\varphi\mu_0)$. In this example, $\varepsilon_r = 3$, $\varepsilon_\theta = \varepsilon_\varphi = 1.5$ and $\mu_r = 1.5$, $\mu_\theta = \mu_\varphi = 3$. For the detailed comparison between the proposed SE-MLFMA (*prop*) and the conventional MLFMA (*conv*), Table 1 shows the influence of L and P on the memory cost (*Mem*) of RPs or ECs and the computing time per MVP (T_m), while $L = 5$ or 6 is obtained from 0.2λ or 0.25λ leaf box size obeying the same truncation order [6], respectively. Figure 1 compares the numerical results by using the conventional MLFMA and the SE-MLFMA when 0.2λ leaf box size is adopted with $L = 5$. The exact result from Mie series is also shown for comparison [7], while the RMS errors of *conv* and *prop* compared with the exact result are given in Table 1. It is found that the result from *conv* with $L = 5$ and that from *prop* with $P = 2$ or 3 show the same accuracy, while $P = 1$ leads to a relatively large error nearby the backward range ($\theta = 0$). This indicates that a moderate multipole truncation order and a commonly leaf box size are enough for the SE-MLFMA.

The second object is a two-layer bi-isotropic sphere, while the radii of inner and outer spherical surfaces are 0.4λ and 0.5λ, and the medium parameters of inner and outer are $\overline{\overline{\varepsilon}}_{\mathrm{in}} = 1.5\varepsilon_0\overline{\overline{I}}$, $\overline{\overline{\mu}}_{\mathrm{in}} = \mu_0\overline{\overline{I}}$, $\overline{\overline{\xi}}_{\mathrm{in}} = \overline{\overline{\zeta}}^{*}_{\mathrm{in}} = 0$ and $\overline{\overline{\varepsilon}}_{out} = 2\varepsilon_0\overline{\overline{I}}$, $\overline{\overline{\mu}}_{out} = \mu_0\overline{\overline{I}}$, $\overline{\overline{\xi}}_{out} = \overline{\overline{\zeta}}^{*}_{\mathrm{out}} = (0.5 - j0.5)\sqrt{\varepsilon_0\mu_0}\overline{\overline{I}}$, respectively. This object is illuminated by an EM plane wave from

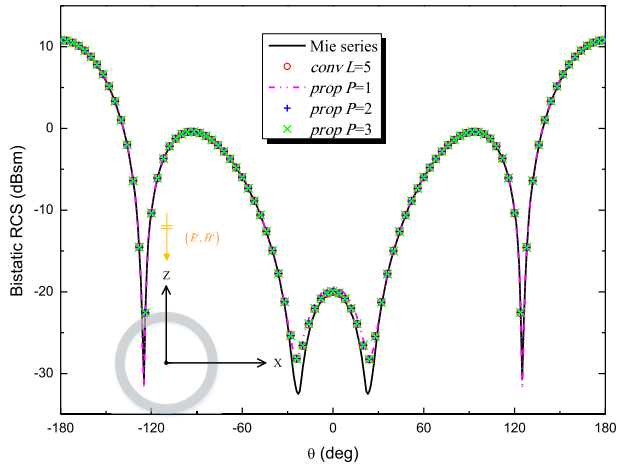

FIGURE 1. Bistatic RCS for a 0.055 m thick anisotropic shell of 1 m outer radius with $\varepsilon_r = 3$, $\varepsilon_\theta = \varepsilon_\varphi = 1.5$ and $\mu_r = 1.5$, $\mu_\theta = \mu_\varphi = 3$, illuminated by a θ-polarized plane wave at 140 MHz from $+z$ axis, the observation range is at $-180° \leqslant \theta \leqslant 180°$ in xz plane. "*conv*" is for the conventional implementation of MLFMA, "*prop*" is for the proposed approach.

TABLE 1. Memory requirement by RPs and CPU time per iteration with respect to various of L and P.

	Method	*conv*, L=5	*prop*, L=5		
			P=1	P=2	P=3
spherical shell	*Mem* (MB)	64.76	5.40	10.79	17.99
	R_M	—	12.0	6.0	3.6
	T_m (sec)	1.52	0.901	0.995	1.13
	RMS (dB)	0.69	0.95	0.71	0.70
	Method	*conv*, L=6	*prop*, L=6		
			P=1	P=2	P=3
	Mem (MB)	88.14	5.40	10.79	17.99
	R_M	—	16.3	8.2	4.9
	T_m (sec)	2.376	1.67	1.82	2.01
	RMS (dB)	0.68	1.02	0.71	0.70
two-layer sphere	Method	*conv*, L=5	*prop*, L=5		
			P=1	P=2	P=3
	Mem (MB)	239.7	19.98	39.95	66.58
	R_M	—	12.0	6.0	3.6
	T_m (sec)	18.39	10.21	13.43	16.45
	RMS(dB) $\theta\theta$	0.24	0.53	0.26	0.25
	RMS(dB) $\varphi\varphi$	0.27	0.60	0.29	0.29
	RMS(dB) $\theta\varphi$	0.17	0.49	0.17	0.16
	RMS(dB) $\varphi\theta$	0.13	0.46	0.15	0.14
cylinder	Method	*conv*, L=5	*prop*, L=5		
			P=1	P=2	P=3
	Mem (MB)	24.68	2.06	4.11	6.86
	R_M	—	12.0	6.0	3.6
	T_m (sec)	0.445	0.254	0.298	0.337
comb.	Method	*conv*, L=5	*prop*, L=5		
			P=1	P=2	P=3
	Mem (MB)	1561.5	130.1	260.2	433.8
	R_M	—	12.0	6.0	3.6
	T_m (sec)	79.3	59.8	65.7	71.1

$-z$-axis, and the observation range is $0 \leqslant \theta \leqslant 180°$ and $\varphi = 0$. After the discretization, the numbers of tetrahedrons and unknowns are 43,033 and 175,152, respectively, with an average mesh size 0.07λ. The material is modeled by two-layer tetrahedral meshes. The numerical results from *conv* ($L = 5$) and *prop* ($P = 2$) as well as exact results from [9] are shown in Fig. 2, while good agreements are observed. The performance details as well as the RMS error results are shown in Table 1. It is found that for the $\theta\varphi$-polarization,

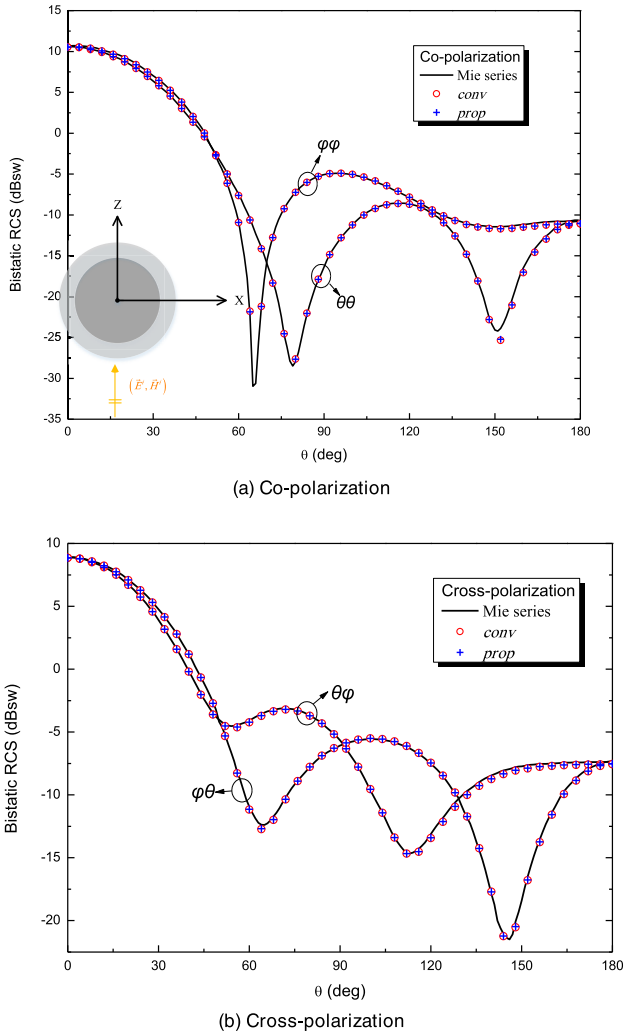

FIGURE 2. Bistatic RCS for a two-layer sphere with inner and outer radii of 0.4λ and 0.5λ, illuminated by a θ-polarized plane wave from $-z$ axis; the inner and outer medium parameters are $\bar{\bar{\varepsilon}}_{in} = 1.5\varepsilon_0\bar{\bar{I}}$, $\bar{\bar{\mu}}_{in} = \mu_0\bar{\bar{I}}$, $\bar{\bar{\xi}}_{in} = \bar{\bar{\zeta}}^*_{in} = 0$ and $\bar{\bar{\varepsilon}}_{out} = 2\varepsilon_0\bar{\bar{I}}$, $\bar{\bar{\mu}}_{out} = \mu_0\bar{\bar{I}}$, $\bar{\bar{\xi}}_{out} = \bar{\bar{\zeta}}^*_{out} = (0.5 - j0.5)\sqrt{\varepsilon_0\mu_0}\bar{\bar{I}}$.

the proposed SE-MLFMA with $P = 3$ shows 0.01 dB reduction in the RMS error difference compared with the conventional MLFMA. Under the mesh size and iterative solver adopting by this example, this 0.01 dB may be consistent with the accuracy of computation.

The third object is a homogeneous bi-anisotropic cylinder with 0.5λ radius and 0.2λ height, illuminated by an EM plane wave from -z-axis, and the observation range is $0 \leqslant \theta \leqslant 180°$ and $\varphi = 0$. The medium parameters are $\bar{\bar{\varepsilon}} = \text{diag}(2\varepsilon_0, 3\varepsilon_0, 2\varepsilon_0)$, $\bar{\bar{\mu}} = \text{diag}(1.2\mu_0, 1.2\mu_0, \mu_0)$, while for $\bar{\bar{\xi}}$ and $\bar{\bar{\zeta}}$, $\xi_{21} = \zeta^*_{12} = -j\Omega\sqrt{\varepsilon_0\mu_0}$ and other elements are zero. A 0.07λ mesh size is set to generate totally 18,072 unknowns with 4,395 tetrahedrons. Numerical results from *conv* ($L = 5$) and *prop* ($P = 2$) are shown in Fig. 3, while the results from [22] (ref) implemented by Y. Zhang *et al.* using the finite element-boundary integral method are also given for comparison. With different Ω, the $\theta\theta$-polarization results are

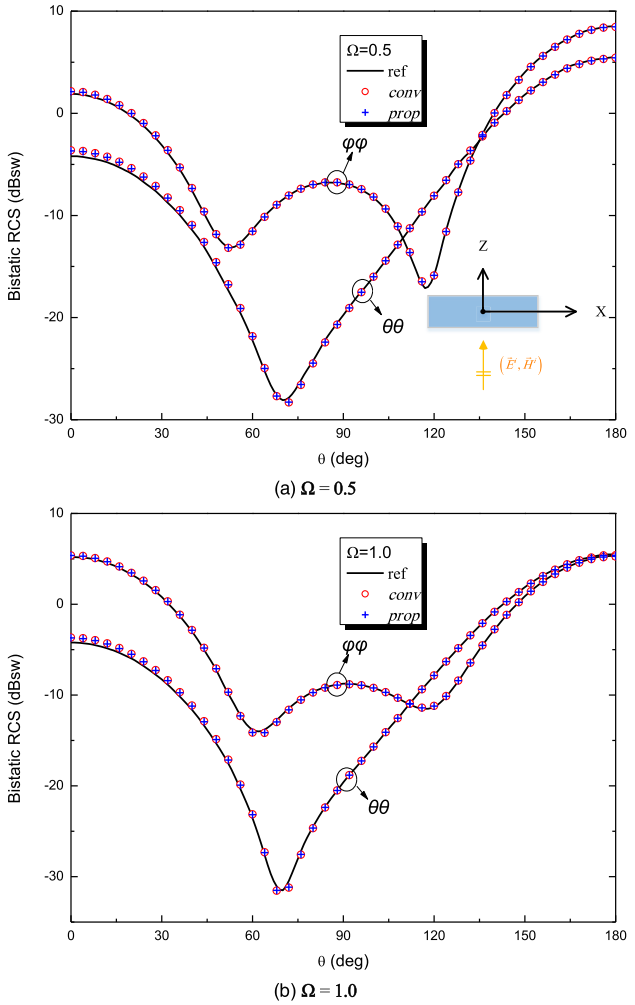

FIGURE 3. Bistatic RCS for a homogeneous bi-anisotropic cylinder with 0.5λ radius and 0.2λ tall, illuminated by an EM plane wave from $-z$-axis.

similar, while the $\varphi\varphi$-polarization changes a lot. The performance details are shown in Table 1.

In the fourth, we consider a combinative structure of four different objects, placing along the y direction in order, as shown in Fig. 4. The center distance between two neighbor objects is 3λ. For easy presentation, we define

$$\bar{\bar{\Lambda}} = \begin{bmatrix} 2.5 & -j & 0 \\ j & 2.5 & 0 \\ 0 & 0 & 1.5 \end{bmatrix} \tag{33}$$

The first object is a $2\lambda \times 2\lambda \times 0.2\lambda$ size of gyromagnetic cube with $\bar{\bar{\varepsilon}}_1 = \varepsilon_0 \bar{\bar{\Lambda}}$. The second one is a Faraday chiral almond [23] shell with $\bar{\bar{\varepsilon}}_2 = \varepsilon_0 \bar{\bar{\Lambda}}$, $\bar{\bar{\mu}}_2 = \mu_0 \bar{\bar{\Lambda}}$, $\bar{\bar{\xi}}_2 = \bar{\bar{\zeta}}_2^* = (0.5 - j0.5)\sqrt{\varepsilon_0\mu_0}\bar{\bar{I}}$. The outer length is 3λ with a 0.1λ thick shell. The third one is a chiral spherical shell with $\bar{\bar{\varepsilon}}_3 = (2 - j2)\varepsilon_0\bar{\bar{I}}$, $\bar{\bar{\mu}}_3 = (2 - j2)\mu_0\bar{\bar{I}}$, $\bar{\bar{\xi}}_3 = \bar{\bar{\zeta}}_3^* = (0.5 - j0.5)\sqrt{\varepsilon_0\mu_0}\bar{\bar{I}}$. The outer radius is 1.55λ, while the shell thickness is 0.05λ. The last one is a gyroelectric cylinder with $\bar{\bar{\mu}}_4 = \mu_0\bar{\bar{\Lambda}}$, whose radius and height are 1λ and 0.2λ, respectively. After discretizing, the numbers of tetrahedrons and unknowns are 268,560 and 1,152,684 with 0.05λ average

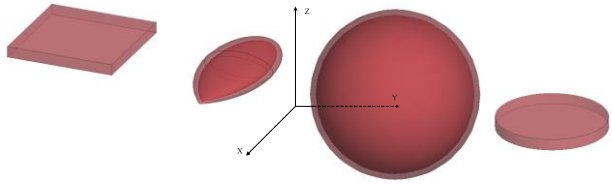

FIGURE 4. Position of the combination in the Cartesian coordinate.

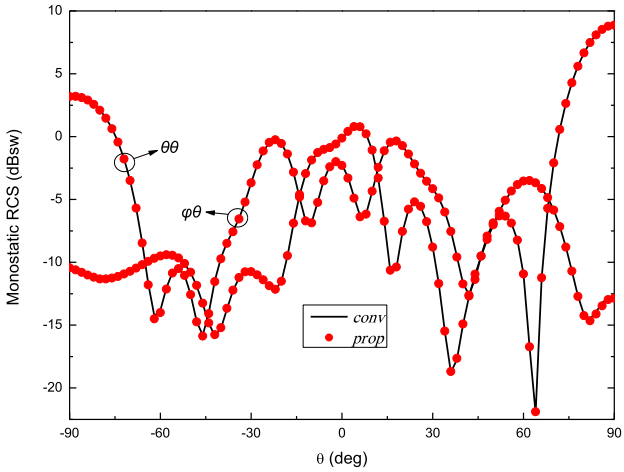

FIGURE 5. Monostatic RCS for a combination of four different objects, the observation range is at $-90° \leq \theta \leq 90°$ and $\varphi = 0$.

mesh size, respectively. Monostatic RCS at $-90° \leqslant \theta \leqslant 90°$ and $\varphi = 0$ is calculated, while the performance details and numerical results are shown in Table 1 (comb.) and in Fig. 5, respectively. It is found that due to the general medium tensor parameters, the cross-polarization ($\varphi\theta$) and the co-polarization ($\theta\theta$) have the same level in most angles, which cannot be ignored. However, for $\theta = \pm 90°$, the cross-polarization is much lower than its counterpart.

From Table 1, it is observed that due to the use of SE-MLFMA, a considerable core memory is saved, while the memory requirement of RPs or ECs and R_M rigidly match with (29)-(31). Besides, the value of R_M is only relative to L and P and independent of the shape of object, which demonstrates that (31) is suitable for all kinds of cases. Moreover, the SE-MLFMA is more efficient than the conventional one during the MVP implementation, since the aggregation of the outgoing waves and the disaggregation of the incoming waves at the finest level can also be executed in a faster way by fully utilizing the orthonormality of the spherical harmonics.

V. CONCLUSION

The SE-MLFMA is proposed and successfully implemented to solve the EM scattering by inhomogeneous bi-anisotropic objects. With a mixed-potential VIE representation and the tetrahedron-based grouping scheme, rather than the commonly used dyadic form and face-based scheme, a considerable amount of core memory requirement of RPs is reduced without compromising accuracy. In addition, elimination of the transformations of RPs between the spherical and Cartesian coordinates yields a faster computation. Great flexibility of the method is exhibited through the numerical examples.

REFERENCES

[1] A. Serdyukov, I. Semchenko, S. Tretyakov, and A. Sihvola, *Electromagnetics of Bi-anisotropic Materials: Theory and Applications*. New York, NY, USA: Gordon and Breach, 2001.

[2] S. G. Johnson and J. D. Joannopoulos, *Photonic Crystals: The Road from Theory to Practice*. Boston, MA, USA: Kluwer, 2002.

[3] P. A. Belov and C. R. Simovski, "Analytical modelling of semi-infinite electromagnetic crystal's excitation by plane electromagnetic wave," in *Proc. IEEE Antennas Propag. Soc. Symp.*, Monterey, CA, USA, vol. 4, 2004, pp. 3781–3784.

[4] E. Yablonovitch, "Photonic band-gap structures," *J. Opt. Soc. Amer. B, Opt. Phys.*, vol. 10, no. 2, pp. 283–295, 1993.

[5] R. F. Harrington, *Field Computation by Moment Methods*. New York, NY, USA: Macmillan, 1968.

[6] W. C. Chew, J. M. Jin, E. Michielssen, and J. M. Song, *Fast and Efficient Algorithms in Computational Electromagnetics*. Boston, MA, USA: Artech House, 2001.

[7] G. Kobidze and B. Shanker, "Integral equation based analysis of scattering from 3-D inhomogeneous anisotropic bodies," *IEEE Trans. Antennas Propag.*, vol. 52, no. 10, pp. 2650–2658, Oct. 2004.

[8] L. Hu, L.-W. Li, and T. S. Yeo, "Analysis of scattering by large inhomogeneous bi-anisotropic objects using AIM," *Prog. Electromagn. Res.*, vol. 99, pp. 21–36, 2009.

[9] D. X. Wang, E. K. N. Yun, R. S. Chen, and P. Y. Lau, "An efficient volume integral equation solution to EM scattering by complex bodies with inhomogeneous bi-isotropy," *IEEE Trans. Antennas Propag.*, vol. 55, no. 7, pp. 1970–1981, Jul. 2007.

[10] J. Markkanen, P. Yla-Oijala, and A. Sihvola, "Discretization of volume integral equation formulations for extremely anisotropic materials," *IEEE Trans. Antennas Propag.*, vol. 60, no. 11, pp. 5195–5202, Nov. 2012.

[11] J. Liu, Z. Li, J. Su, and J. Song, "On the volume-surface integral equation for scattering from arbitrary shaped composite PEC and inhomogeneous bi-isotropic objects," *IEEE Access*, vol. 7, pp. 85594–85603, 2019.

[12] Y.-N. Liu, X.-M. Pan, and X.-Q. Sheng, "Skeletonization accelerated MLFMA solution of volume integral equation for plasmonic structuress," *IEEE Trans. Antennas Propag.*, vol. 66, no. 3, pp. 1590–1594, Mar. 2018.

[13] X.-M. Pan, W.-C. Pi, M.-L. Yang, Z. Peng, and X.-Q. Sheng, "Solving problems with over one billion unknowns by the MLFMA," *IEEE Trans. Antennas Propag.*, vol. 60, no. 5, pp. 2571–2574, May 2012.

[14] Z. He, J. H. Gu, W. E. I. Sha, and R. S. Chen, "Efficient volumetric method of moments for modeling plasmonic thin-film solar cells with periodic structures," *Opt. Express*, vol. 26, no. 19, pp. 25037–25046, 2018.

[15] T. F. Eibert, "A diagonalized multilevel fast multipole method with spherical harmonics expansion of the k-space Integrals," *IEEE Trans. Antennas Propag.*, vol. 53, no. 2, pp. 814–817, Feb. 2005.

[16] M. He, J. Liu, and K. Zhang, "Improving the spherical harmonics expansion-based multilevel fast multipole algorithm (SE-MLFMA)," *IEEE Antennas Wireless Propag. Lett.*, vol. 12, pp. 551–554, 2013.

[17] D. H. Schaubert, D. R. Wilton, and A. W. Glisson, "A tetrahedral modeling method for electromagnetic scattering by arbitrarily shaped inhomogeneous dielectric bodies," *IEEE Trans. Antennas Propag.*, vol. AP-32, no. 1, pp. 77–85, Jan. 1984.

[18] D. Wilton, S. Rao, A. Glisson, D. Schaubert, O. Al-bundak, and C. Butler, "Potential integrals for uniform and linear source distributions on polygonal and polyhedral domains," *IEEE Trans. Antennas Propag.*, vol. 32, no. 3, pp. 276–281, Mar. 1984.

[19] M. G. Duffy, "Quadrature over a pyramid or cube of integrands with a singularity at a vertex," *SIAM J. Numer. Anal.*, vol. 19, no. 6, pp. 1260–1262, 1982.

[20] R. F. Harrington, *Time-Harmonic Electromagnetic Fields*. New York, NY, USA: McGraw-Hill, 1961.

[21] S. Koc, J. Song, and W. C. Chew, "Error analysis for the numerical evaluation of the diagonal forms of the scalar spherical addition theorem," *SIAM J. Numer. Anal.*, vol. 38, no. 3, pp. 906–921, 1999.

[22] Y. Zhang, X. Wei, and E. Li, "Electromagnetic scattering from three-dimensional bianisotropic objects using hybrid finite element-boundary integral method," *J. Electromagn. Waves Appl.*, vol. 18, no. 11, pp. 1549–1563, 2004.

[23] A. C. Woo, H. T. G. Wang, M. J. Schuh, and M. L. Sanders, "EM programmer's notebook-benchmark radar targets for the validation of computational electromagnetics programs," *IEEE Trans. Antennas Propag.*, vol. 35, no. 1, pp. 84–89, Feb. 1993.

JINBO LIU received the B.S. degree in electronic information engineering from Zhengzhou University, Zhengzhou, China, in 2010, and the Ph.D. degree in electronic science and technology from the Beijing Institute of Technology, Beijing, China, in 2016.

He is currently an Associate Professor with the School of Information and Communication Engineering, Communication University of China, Beijing. His current research interests include computational electromagnetics, parallel computation, and numerical analysis of antenna array.

ZENGRUI LI received the B.S. degree in communication and information system from Beijing Jiaotong University, Beijing, China, in 1984, the M.S. degree in electrical engineering from the Beijing Broadcast Institute, Beijing, in 1987, and the Ph.D. degree in electrical engineering from Beijing Jiaotong University, in 2009.

He studied at Yokohama National University, Yokohama, Japan, from 2004 to 2005. He is currently a Professor with the School of Information and Communication Engineering, Communication University of China, Beijing. His research interests include the areas of finite-difference time-domain (FDTD) methods, electromagnetic scattering, metamaterials, and antennas.

Prof. Li is a Senior Member of the Chinese Institute of Electronics.

LIMEI LUO received the B.S. degree in communication engineering from Fuzhou University, Fuzhou, China, in 2004, and the M.S. degree in electrical engineering from the Communication University of China, Beijing, China, in 2007, where she is currently pursuing the Ph.D. degree in electromagnetics and microwave technology.

Her current research interests include computational electromagnetics, metamaterials, and antennas.

JIMING SONG (S'92–M'95–SM'99–F'14) received the B.S. and the M.S. degrees in physics from Nanjing University, China, in 1983 and 1988, respectively, and the Ph.D. degree in electrical engineering from Michigan State University, East Lansing, MI, USA, in 1993.

From 1993 to 2000, he was a Postdoctoral Research Associate, a Research Scientist, and a Visiting Assistant Professor with the University of Illinois at Urbana–Champaign. From 1996 to 2000, he worked part-time as a Research Scientist with SAIC-DEMACO. He was the Principal Author of the *Fast Illinois Solver Code* (FISC). He was a Principal Staff Engineer/Scientist with Semiconductor Products Sector of Motorola, Tempe, Arizona, before he joined the Department of Electrical and Computer Engineering, Iowa State University, as an Assistant Professor, in 2002, where he currently is a Professor with the Department of Electrical and Computer Engineering, and a Visiting Professor with the School of Information and Communication Engineering, Communication University of China, Beijing, China. His research has dealt with modeling and simulations of interconnects on lossy silicon and RF components, electromagnetic wave scattering using fast algorithms, the wave propagation in metamaterials, acoustic and elastic wave propagation and non-destructive evaluation, and transient electromagnetic field. He was selected as a National Research Council/Air Force Summer Faculty Fellow, in 2004 and 2005. He was a recipient of the NSF Career Award, in 2006. He is also an ACES Fellow and an Associate Editor for the IEEE ANTENNAS AND WIRELESS PROPAGATION LETTERS (AWPL) and ACES Express.